JOURNAL OF MAGNETIC RESONANCE **124,** 72–79 (1997)
ARTICLE NO. MN967483

Adiabatic Slice-Selective Excitation for Surface Coils

JUN SHEN*,† AND DOUGLAS L. ROTHMAN‡

*Magnetic Resonance Center, *Department of Molecular Biophysics and Biochemistry, and ‡Internal Medicine, Yale University School of Medicine, New Haven, Connecticut 06510*

Received June 28, 1996; revised September 9, 1996

A novel RF pulse designed to perform *a*diabatic *s*lice-*s*elective *e*xcitation for *s*urface coil*s* (ASSESS) is proposed in which B_0 gradient is modulated in concert with RF frequency modulation. Within the selected slice, the principles of BIR4 pulses are employed to obtain well-defined, pure-phase and self-refocused spin rotation of arbitrary flip angles despite the presence of high B_1 inhomogeneity produced by surface coils. Outside the slice, advantage is taken of the B_1 field to dephase equilibrium magnetization to achieve slice selection or outer-volume suppression. This scheme should be useful for many localization techniques. Quaternion analysis of the overall propagator of the proposed pulse and numerical simulations using Bloch equations are performed. The pulse is tested experimentally on a phantom sample.

INTRODUCTION

The high sensitivity and restricted field of view of surface coils have made them an important tool in *in vivo* spectroscopy and imaging. A limitation of surface coils is their high B_1 inhomogeneity, which makes them unsuitable as RF transmission coils for many RF pulses and multipulse sequences, the performance of which degrades significantly in the presence of B_1 inhomogeneity. Such limitations have stimulated the design of various adiabatic pulses which can induce well-behaved spin transformations when surface coils are used for RF transmission. Many efforts have been made to design adiabatic pulses for selective inversion (*1*) and refocusing (*2*), nonselective excitation (*3, 4*), refocusing (*5*), and universal rotations of arbitrary flip angles (*6*).

The development of a slice-selective adiabatic excitation pulse, although very desirable in spatial localization and two-dimensional imaging, has been elusive. Few attempts have been made since the introduction to Fourier transform NMR of efficient adiabatic sweep pulses more than 10 years ago (*7*). Johnson *et al.* (*8*) first proposed a gradient-modulated adiabatic excitation (GMAX) pulse. With a temporally modulated B_0 gradient and a NOM pulse (*3*), slice selection is achieved using a single pulse, but with a minimum of two scans. A sign switching of frequency or gradient modulation for alternate scans is needed. The main drawback of this method is that, due to the need for subtraction, motion, or other instabilities will lead to contamination by magnetization outside the selected slice. Perturbation of equilibrium magnetization outside the slice also makes multislice imaging impossible. Saranathan and Kushmerick (*9*) proposed to replace each segment of a DANTE pulse (*10*) with small-flip-angle BIR4 pulses (*6*) to obtain frequency-selective adiabatic excitation. At least 10 BIR4 pulses [i.e., 40 adiabatic half-passage (AHP) pulses] are needed to generate reasonably selective excitation. Excessive RF power deposition is unavoidable with this approach. de Graaf *et al.* (*11*) combined the GMAX and BIR pulses and proposed a single-shot, adiabatic, universal-rotator pulse of arbitrary flip angles for surface-coil applications (BISS8). Magnetization outside the slice is not perturbed. This is an ideal pulse except that the requirements of eight adiabatic half-passage pulses cause significant RF power deposition and long pulse duration, and the need for abrupt gradient switching at its maximum strength complicates its implementation due to finite gradient slew rate. All these have limited its practical usage and quality of experimental performance (*11*).

In this paper, we propose a new approach to the design of slice-selective adiabatic excitation pulses (ASSESS) combining the GMAX and BIR4 pulses. An unmodified BIR4 pulse is applied during the presence of temporal B_0 modulation and spatial B_1 inhomogeneity. Only four AHP pulses are required. No abrupt gradient switching is necessary. Well-defined slice profiles are obtained experimentally. In our approach, magnetization outside the selected slice is dephased by the B_1 field. Therefore, interleaved multiple-slice imaging is not possible. However, we believe that the relatively low RF power requirements as well as excellent experimental performance of this pulse make it a good candidate for practical implementation. Modifications of the ASSESS pulse to avoid perturbation of magnetization outside the chosen slice or to achieve complete suppression of magnetization outside the slice regardless of the B_1 homogeneity will also be discussed.

† To whom correspondence should be addressed.

1090-7807/97 $25.00

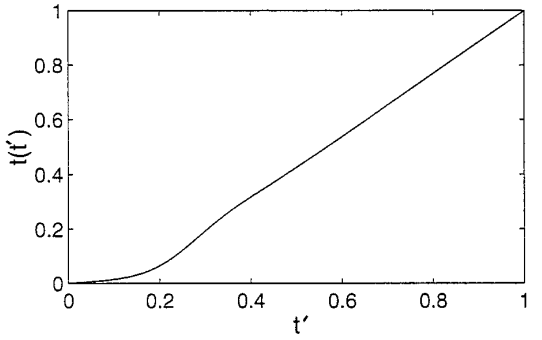

FIG. 1. $t(t')$ vs t' obtained from the modified NOM procedure described in Refs. (*8, 11*) using tanh/sech as the starting functions for amplitude and frequency/gradient modulations. The adiabatic half-passage pulse (AHP) is optimized for the $\nu(\mathbf{r})$ range of 0.2 ~ 5 and the $g_0(\mathbf{r})$ range of 1.5 ~ 12.5 as described in the text.

THEORY

We describe the ASSESS pulse in the frequency-modulated (FM) frame (*12*). The basic components of the ASSESS pulse (an AHP pulse) are described by the equations

$$B_1(\mathbf{r}, t) = \nu(\mathbf{r})AF_1(t) \quad [1]$$

$$\omega(t) = AF_2(t) \quad [2]$$

$$G(\mathbf{r}, t) = g_0(\mathbf{r})AF_2(t), \quad [3]$$

where $B_1(\mathbf{r}, t)$ is the RF amplitude as a function of spatial location and time, $\omega(t)$ is the RF frequency modulation, $G(\mathbf{r}, t)$ is the gradient modulation in the dimension of frequency, $\nu(\mathbf{r})$ is the normalized B_1 spatial inhomogeneity factor $[=B_{1\max}(\mathbf{r})/A]$, A is the amplitude of frequency modulation, $g_0(\mathbf{r})$ is the signed normalized gradient factor $[=G_{\max}(\mathbf{r})/A]$, $F_1(t)$ is the dimensionless RF amplitude-modulation function starting from zero and growing to unity, and $F_2(t)$ is the dimensionless RF frequency and gradient amplitude-modulation function starting from unity and decaying to zero. The adiabatic half-passage pulse duration is T.

As discussed previously (*8, 11*), many different $F_1(t)$ and $F_2(t)$ modulation functions (e.g., the tanh/sech pair) can be used. However, better performance is obtainable using the modified NOM procedure (*8, 11*) including time-dependent resonance-offset terms produced by the B_0 gradient modulation. The following parameters are used for simulation and experimental test in this study: $T = 5$ ms, $A = 4000$ Hz. The pulse is optimized for $\nu(\mathbf{r}) = 0.2{-}5$, $g_0(\mathbf{r}) = 1.5{-}12.5$. The optimization procedure is similar to that given in Refs. (*8, 11*) using the tanh/sech pair as the trial functions. The resulting time-substitution function $t(t')$ vs t' is plotted in Fig. 1.

The four-segment ASSESS pulse is given in Fig. 2 with its cancatenation of RF amplitude, frequency, and phase modulations identical to a standard BIR4 pulse. The phase modulation $\phi(t)$ has two discontinuous phase shifts defined by

$$\Delta\phi_1 = -\Delta\phi_2 = 180° + \theta/2. \quad [4]$$

The in-slice flip angle is θ. The gradient modulation is identical to the frequency modulation except the polarity of the gradient is unchanged during the pulse.

In the FM frame, the effect of frequency modulation appears as an additional resonance offset given by $\omega(t)$ (*12*); the total apparent resonance offset during the execution of the ASSESS pulse in the absence of chemical-shift offset and B_0 inhomogeneity is therefore

$$\Delta\omega(\mathbf{r}, t) = [g_0(\mathbf{r}) - 1]AF_2(t). \quad [5]$$

The slice thickness is defined by $g_0(\mathbf{r}) = \pm 1$. Within the selected slice, the RF frequency modulation dictates the sign of $\Delta\omega(\mathbf{r}, t)$; thus, an exact BIR4 rotation of θ degrees is obtained after the ASSESS pulse. It is important to note that, for such a rotation, the overall rotation angle and the position of the overall rotation axis are fixed regardless of the resonance offset (or spatial position for gradient-induced resonance offset). This will be demonstrated below by calculation of the quaternions of ASSESS pulses.

It has been shown previous (*13, 14*) that composite rotations can be conveniently described by the quaternion elements of their overall propagator, which allows an evaluation of the position of the overall rotation axes as well as the overall rotation angle regardless of the initial position of the magnetization. As given by Emsley and Bodenhausen (*15*), the quaternions of the overall propagator are related to the net rotation angle θ and the position of the overall rotation axis by

$$\mathbf{A} = -l_{xx}\sin(\theta/2) \quad [6]$$

$$\mathbf{B} = -l_{yy}\sin(\theta/2) \quad [7]$$

$$\mathbf{C} = -l_{zz}\sin(\theta/2) \quad [8]$$

$$\mathbf{D} = \cos(\theta/2), \quad [9]$$

where l_{xx}, l_{yy}, and l_{zz} are directional cosines of the overall rotation axis. The quaternions of the 90° ASSESS pulse depicted in Fig. 2 at $\nu(\mathbf{r}) = 1$ in the phase-modulated (PM) frame (*12*) are given in Fig. 3.

As shown in Fig. 3, the overall rotation axis is along the x axis regardless of the variation in resonance offset induced by the B_0 gradient except for the two narrow transition regions. This is indicated by the fact that $\mathbf{B} = \mathbf{C} = 0$. The net rotation angle is 90° within the selected slice $[-1 < g_0(\mathbf{r})$

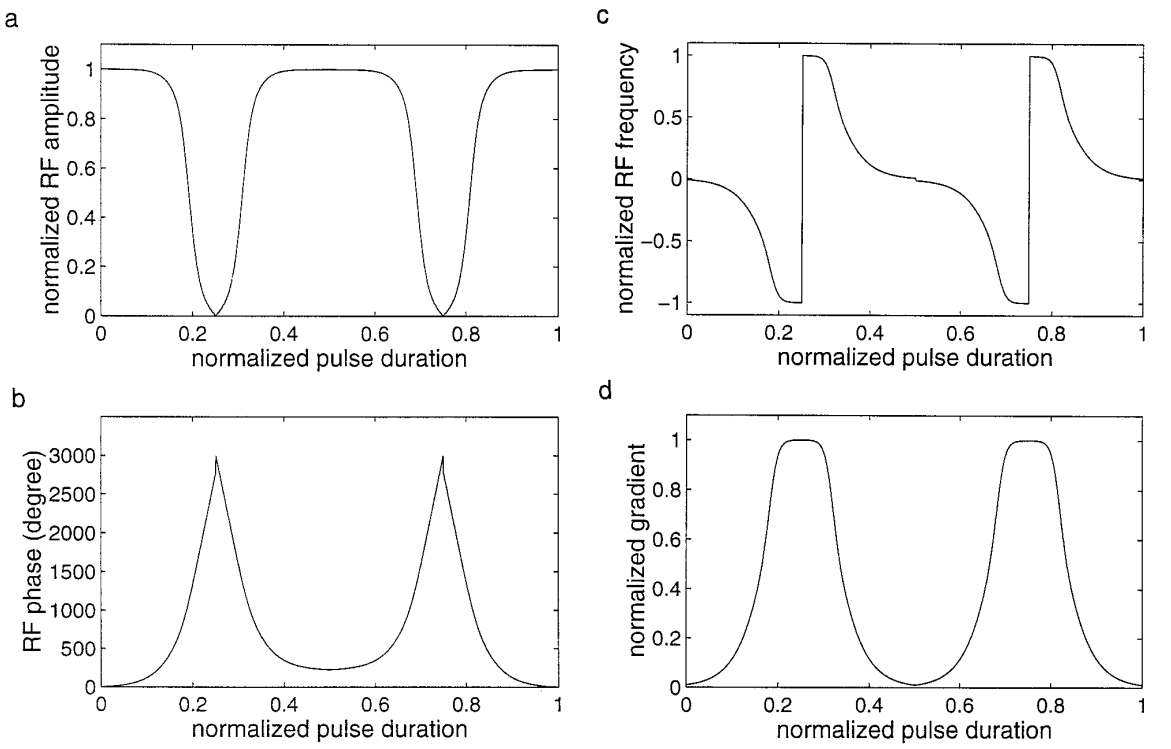

FIG. 2. RF amplitude (a), phase (b), frequency (c), and B_0 gradient (d) modulations as a function of sample points of the ASSESS pulse. The RF amplitude, frequency, and B_0 gradient are normalized to A. The RF phase (instead of frequency) modulation is in the units of degrees. The pulse is implemented according to the RF amplitude and phase modulations shown above. The desired flip angle is generated by the two discontinuous phase shifts defined by Eq. [4]. The modulation functions shown are optimized to perform adiabatically over a predefined range of $\nu(\mathbf{r})$ ($0.2 \sim 5$) and $g_0(\mathbf{r})$ ($1.5 \sim 12.5$). $A = 4$ kHz, $T = 5$ ms, $\theta = \pi/2$.

< 1], where $\mathbf{A} = -\sin(\pi/4)$, $\mathbf{D} = \cos(\pi/4)$. Outside the slice, the net rotation angle varies with resonance offset. This is confirmed by the Bloch simulations on equilibrium magnetization (data not shown). Within the slice $M_x = M_z = 0$ and $M_y = 1$, while outside the slice $M_x = 0$, M_y and M_z vary between -1 and $+1$. It first appears that such a pulse is of little use due to its ''poor'' performance outside the selected slice. However, when acting on equilibrium magnetization, the effective field produced by the ASSESS pulse is perpendicular to the magnetization throughout the whole duration of the pulse as is the case for a conventional BIR4 pulse. Dephasing during one segment of the pulse is (5)

$$|\phi(\mathbf{r})| = \int_0^T \|\mathbf{B}_{\text{eff}}(\mathbf{r}, t)\| dt, \qquad [10]$$

where

$$\mathbf{B}_{\text{eff}}(\mathbf{r}, t) = [B_1(\mathbf{r}, t), 0, \Delta\omega(\mathbf{r}, t)]. \qquad [11]$$

Within the selected slice, dephasing due to B_1 inhomogeneity produced by a surface transmission coil during segments one and two is refocused during segment three and four, respectively. This is accomplished by the sign changes of $\Delta\omega(\mathbf{r}, t)$ defined by Eq. [5] and the changes of the direction of frequency sweep shown in Fig. 2. Although chemical shift and B_0 inhomogeneity terms are not included in Eq. [5] for simplicity, it can be shown that the rotations caused by the overall effective field, including chemical shift and B_0 inhomogeneity terms during segments one and two, is also refocused for in-slice magnetization by the corresponding rotations during segment three and four. Outside the slice, the preservation of the polarity of the gradient ensures that a sign switch of $\Delta\omega(\mathbf{r}, t)$ does not occur. Therefore, dephasing by B_1 spatial inhomogeneity is accumulated rather than refocused. In addition, the oscillation of the sign of the magnetization outside the selected slice as a function of gradient-induced offset at a constant B_1 produces a dephasing similar to that of a noise pulse. The combination of both dephasing mechanisms leads to excellent suppression of equilibrium magnetization outside the chosen slice. This will be demonstrated experimentally under Experimental.

It should be pointed out that clean slice selection is feasible only when the initial RF field is normal to that of the magnetization. This is possible for equilibrium magnetizations, but it applies only to one component of the transverse

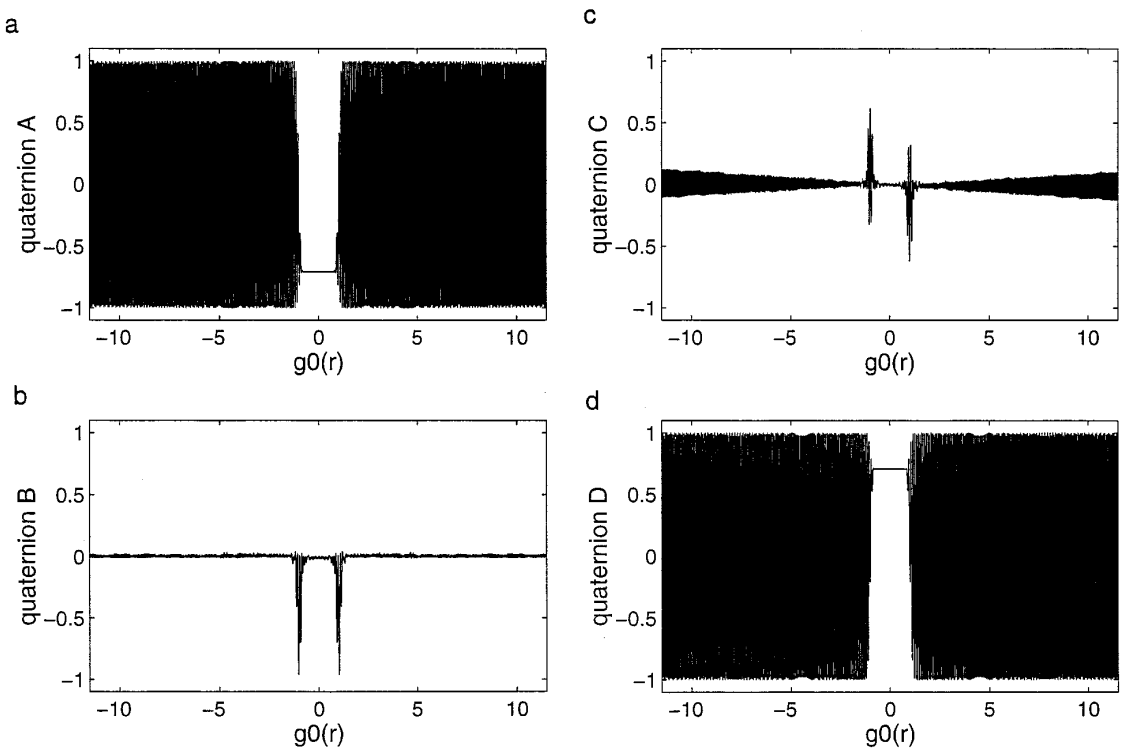

FIG. 3. Quaternion elements of the ASSESS pulse depicted in Fig. 2 as a function of $g_0(\mathbf{r})$ at $\nu(\mathbf{r}) = 1.0$. (a) Quaternion element **A,** (b) quaternion element **B,** (c) quaternion element **C,** and (d) quaternion element **D.** Significant oscillation occurs for quaternions **A** and **D** outside the selected slice as a function of $g_0(\mathbf{r})$ at constant $\nu(\mathbf{r})$.

magnetization. The other component, which is parallel to the B_1 field, will be spin-locked during the entire pulse and will not be dephased by spatial B_1 inhomogeneity produced by a surface transmission coil. Offset slices ($\mathbf{r}_s \neq 0$) can be obtained by modulating the RF pulse with

$$\exp\left[2\pi i \int_t^T g_0(\mathbf{r}_s) A F_2(t)\, dt\right]$$

as a result of the shift theorem given in Ref. (*16*).

Since the AHP pulse employed has been optimized to perform adiabatically over a predefined $g_0(\mathbf{r})$ and a predefined $\nu(\mathbf{r})$ range, we should expect that within the selected slice the ASSESS pulse behaves nearly the same over a certain range of B_1 inhomogeneity, in this case, $\nu(\mathbf{r}) = 0.2 \sim 5$. This is confirmed by quaternion calculations as shown in Fig. 4. Outside the selected slice, the dephasing caused by B_1 inhomogeneity plus oscillation of magnetization along the slice-selection direction ensures the suppression of magnetization as discussed above. In Fig. 4, quaternion elements of the ASSESS pulse depicted in Fig. 2 are calculated as a function of inhomogeneity factor $\nu(\mathbf{r})$ over a range of $0.2 \sim 5$ at $g_0(\mathbf{r}) = 0.0$. As expected, $\mathbf{A} = -\sin(\pi/4)$, $\mathbf{B} = \mathbf{C} = 0$, and $\mathbf{D} = \cos(\pi/4)$ are maintained despite the B_1 inhomogeneity with only small oscillations in **B** visible. Bloch simulations of the final position of the equilibrium magnetization as a function of B_1 inhomogeneity factor $\nu(\mathbf{r})$ over a range of $0.2 \sim 5$ at $g_0(\mathbf{r}) = 0.0$ are performed using the same pulse (data not shown). Essentially, $M_x = M_z = 0$ and $M_y = 1$ are maintained despite the presence of B_1 inhomogeneity with only small oscillations in M_x visible. Bloch simulations of the excitation profile as a function of

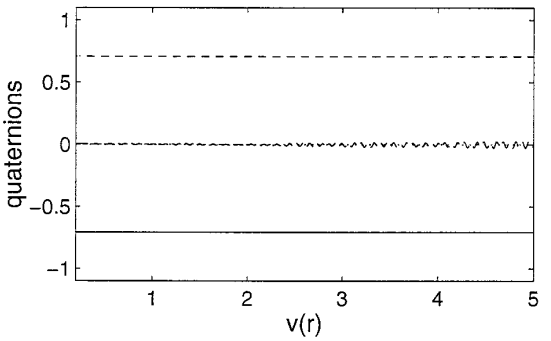

FIG. 4. Quaternion analysis of the ASSESS pulse depicted in Fig. 2 as a function of inhomogeneity factor $\nu(\mathbf{r})$ over a range of $0.2 \sim 5$ at $g_0(\mathbf{r}) = 0.0$. $\mathbf{A} = -\sin(\pi/4)$, $\mathbf{B} = \mathbf{C} = 0$, and $\mathbf{D} = \cos(\pi/4)$ are maintained despite the presence of B_1 inhomogeneity with only small oscillations in quaternion element **B** visible. Solid line, **A;** dotted-dashed, **B;** dotted line, **C;** and dashed line line, **D.**

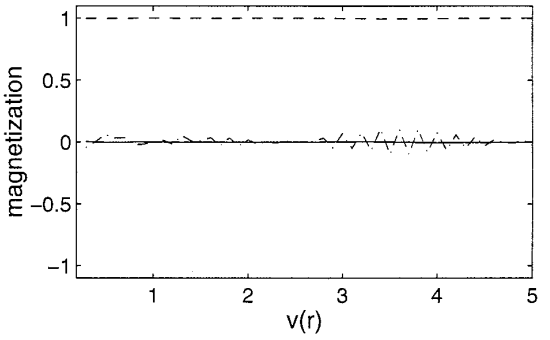

FIG. 5. Bloch simulations of the ASSESS pulse depicted in Fig. 2 as a function of inhomogeneity factor $\nu(\mathbf{r})$ over a range of $0.2 \sim 5$ at $g_0(\mathbf{r}) = 0.5$. $M_x = M_z = 0$ and $M_y = 1$ are maintained despite the presence of B_1 inhomogeneity with marginal oscillations in M_x visible. Dotted-dashed line, M_x; dashed line, M_y; and solid line, M_z.

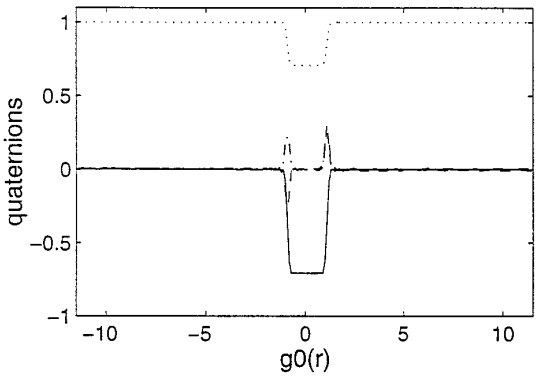

FIG. 6. Quaternion elements of the mASSESS 90° pulse as a function of $g_0(\mathbf{r})$ at $\nu(\mathbf{r}) = 1.0$. The pulse is identical to that depicted in Fig. 2 except the gradient polarity of the second and third segments is reversed. Solid line, quaternion element **A;** dotted-dashed line, quaternion element **B;** dashed line; quaternion element **C;** and dotted line, quaternion element **D.**

$\nu(\mathbf{r})$ over a range of $0.2 \sim 5$ at $g_0(\mathbf{r}) = 0.5$ is shown in Fig. 5. As expected, degradation is only marginal. Similar results are obtained for $-0.6 < g_0(\mathbf{r}) < 0.6$, leading to a very desirable ''top-hat'' slice profile. This is also confirmed experimentally in this study.

If the polarity of the gradient modulation for the second and third segments of the ASSESS pulse is reversed, a true zero rotation outside the selected slice is obtained regardless of B_1 inhomogeneity. Therefore, the magnetization outside the selected slice is not perturbed. Within the selected slice, a BIR4 rotation of arbitrary flip angles similar to that of ASSESS pulse is preserved, except that the rotations caused by the effective field consist of B_0 resonance offset generated by gradient modulation, and possible inhomogeneous B_1 field during each odd-numbered segment are refocused during its subsequent even-numbered segment.

Quaternion calculations of the overall propagator of this *m*odified ASSESS 90° pulse (referred to as mASSESS) are shown in Fig. 6 and the corresponding Bloch simulations of this pulse acting on equilibrium magnetization are shown in Fig. 7. The same pulse parameters as those in Fig. 2 are employed here. It can be seen from Figs. 6 and 7 that the same 90° rotation along the x axis is obtained within the selected slice [as indicated by $\mathbf{A} = -\sin(\pi/4)$, $\mathbf{B} = \mathbf{C} = 0$, and $\mathbf{D} = \cos(\pi/4)$] despite the variation in resonance offset generated by B_0-gradient modulation. Outside the selected slice, the net rotation angle is zero ($\mathbf{A} = \mathbf{B} = \mathbf{C} = 0$, and $\mathbf{D} = 1$) regardless of resonance offset generated by B_0-gradient modulation. Slice selection in this case does not depend on B_1 inhomogeneity. Although $\nu(\mathbf{r}) = 1.0$ is used here, the slice profiles do not degrade with any significance over the predefined $\nu(\mathbf{r})$ range, due to the adiabatic behavior of the AHP components of the mASSESS pulse. There are, however, two distinct drawbacks of the mASSESS pulse which limit its practical usefulness. One is the necessity of abrupt gradient switching at its maximum strength, which complicates its implementation. The other is that, unlike in the case of the ASSESS pulse, nonzero chemical-shift offset and B_0 inhomogeneity, if present, are not refocused here. The slice profile degrades quickly with increasing chemical-shift offset and B_0 inhomogeneity.

An alternative modification explores the symmetry properties of ASSESS pulses. The sign of the frequency response of a $-\theta$ degree and a $180 + \theta$ degree ASSESS pulse relative to that of a θ degree ASSESS pulse is given in Table 1. This is also true in the presence of chemical-shift offset and B_0 inhomogeneity. Therefore, subtraction of two scans produced by a 90° and a −90° ASSESS pulse generates complete suppression of magnetization outside the selected slice independent of the homogeneity of the B_1 field and of chemical-shift offset. The oscillations outside the slice cancel after the subtraction. The results of Bloch simulation using the pulse parameters given in the legend to Fig. 2 are shown in Fig. 8. This scheme is useful for complete outer-volume

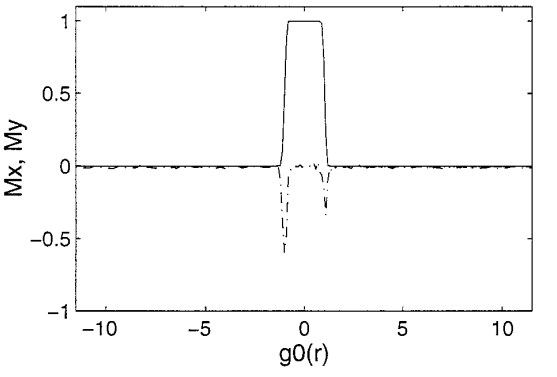

FIG. 7. Bloch simulations of the mASSESS 90° pulse used in Fig. 6 acting on equilibrium magnetization as a function of $g_0(\mathbf{r})$ at $\nu(\mathbf{r}) = 1.0$. Dotted-dashed line, M_x; solid line, M_y.

TABLE 1
Relative Sign Changes of the Frequency Response of ASSESS Pulses Applied along the *x* Axis

	Flip angle					
	θ		$-\theta$		$180° + \theta$	
Slice	In	Out	In	Out	In	Out
M_y	+	+	−	+	−	+
M_z	+	+	+	+	−	+

suppression for *in vivo* spectroscopy where buildup of a useful signal-to-noise ratio requires many scans.

EXPERIMENTAL

To test the performance of the ASSESS pulse, phantom experiments were performed with a 2.1 T Bruker Avance horizontal-bore spectrometer (Bruker Instruments, Billerica, Massachusetts). First, a water-filled cylindrical phantom of 12 cm diameter was placed along the *z* direction on a 7.5-cm-diameter, single-turn surface coil, which was employed for RF transmission and reception. The 90° ASSESS pulse described in Fig. 2 was used for excitation of a slice along *x* axis. The maximum gradient strength available for our spectrometer (2894 Hz/cm or 6.7 mT/m) was used for $G_{0\max}$. This gives a theoretical slice thickness of 2×4000 Hz/2894 Hz/cm = 2.7 cm. The peak RF amplitude was calibrated to generate a 90° rectangular pulse of 25 μs in the coil center (corresponding to a maximum $\nu(\mathbf{r}) = 2.5$). A single-scan gradient echo using a readout gradient along the *x* axis was collected using a gradient strength 40% of $G_{0\max}$ and a FOV of 29 cm. The carrier frequency was set on the resonance of water. The experimental profiles (both absorptive and dispersive modes) are shown in Fig. 9. The measured width at half-height of the profile is 3125 Hz/(40% $\times$ 2894 Hz/cm) = 2.7 cm, which is in excellent agreement with the theoretical prediction. Nearly uniform excitation of magnetization within the selected slice and excellent suppression of magnetization outside the selected slice were obtained with a single scan. No spoiler gradient was used. This confirmed our prediction of the plausibility of slice selection with ASSESS pulses under Theory. The quality of the slice profile compares favorably with that of the BISS8 pulse (*11*). It is also interesting to note that the dispersive component within the two transition regions was not observed experimentally. This is again due to the dephasing caused by B_1 inhomogeneity produced by the surface transmission coil which causes the destructive addition over space of the dispersive signals of the transition regions.

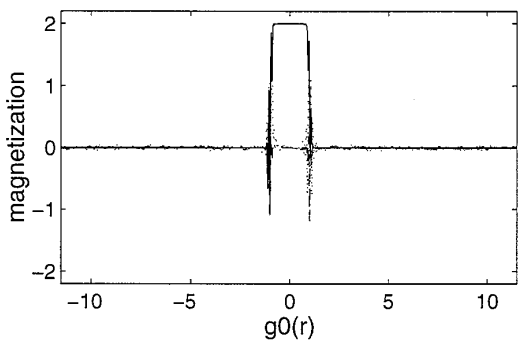

FIG. 8. Bloch simulations of the substraction of two scans generated by a 90° and a −90° ASSESS pulse. The pulse parameters in Fig. 2 with $\nu(\mathbf{r}) = 1.0$ are used. Oscillations in M_y and M_z are cancelled. Dotted line, M_x; solid line, M_y; and dashed line, M_z.

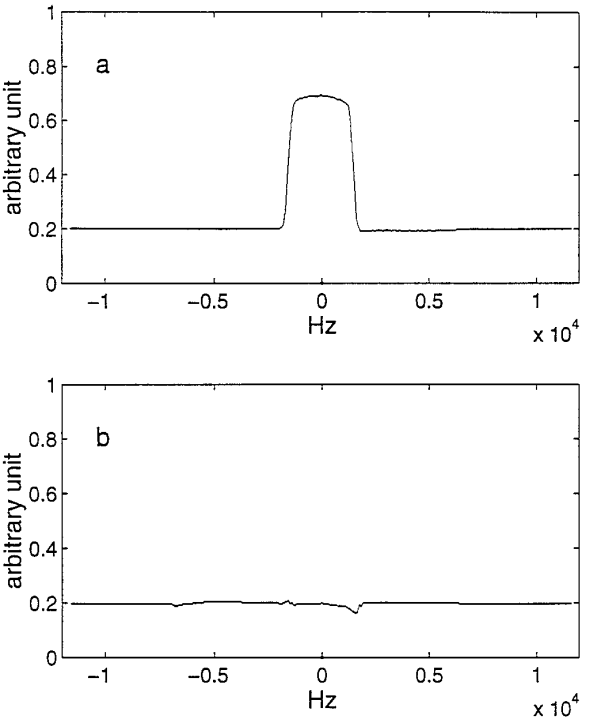

FIG. 9. A gradient-echo slice profile of a water-filled cylindrical phantom produced by the 90° ASSESS excitation pulse depicted in Fig. 2 and a readout gradient along the slice selection direction. A single-turn 7.5 cm surface coil was used for RF transmission and reception. The maximum gradient strength was 6.7 mT/m, giving a slice thickness of 2.7 cm. (a) Absorptive mode; (b) dispersive mode.

Second, to experimentally determine the tolerance of the pulse to B_1, we applied the same ASSESS pulse to select a *z* slice and add a phase-encoding gradient along the *y* axis to acquire a slice image as shown in Fig. 10. As in Fig. 9, a well-defined slice was obtained. This again confirmed the theoretical prediction that the magnetization outside the selected slice is dephased by the high B_1 inhomogeneity produced by the surface transmission coil employed. The decay

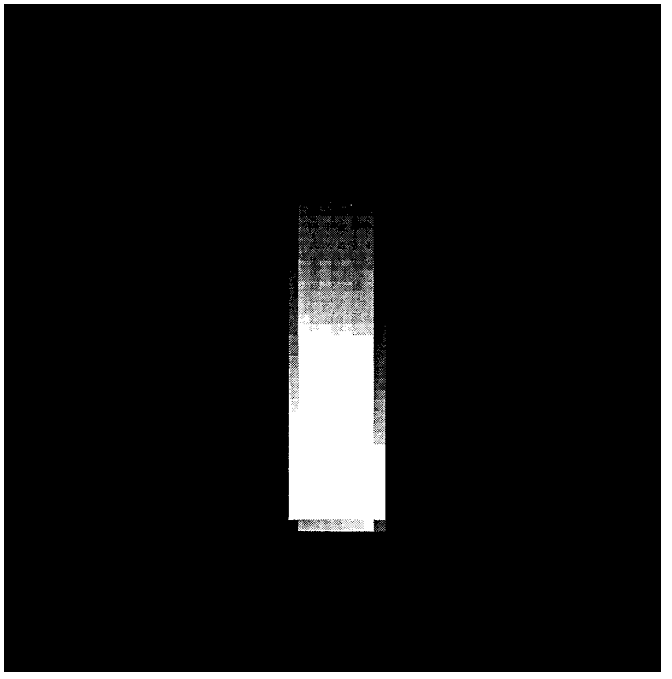

FIG. 10. A z-slice image of the same phantom produced by the 90° ASSESS excitation pulse depicted in Fig. 2. The phase encoding is along y while the slice selection and readout direction are along z. $FOV_z = FOV_y = 43$ cm. The acquisition size is 256×128.

of signal intensity along y is due to unavoidable B_1 dependence of signal detection using surface coils. It is shown in Fig. 10 that the signal intensity decays smoothly with increasing distance from the coil center, indicating uniform excitation despite at least a 10-fold variation in B_1 strength.

Finally, the in-slice image of the slice shown in Fig. 10 was obtained by changing the readout direction from the z axis to the x axis. The result is shown in Fig. 11. Once again, a slice-selective, uniform, adiabatic excitation was obtained despite the presence of the high-B_1 inhomogeneity produced by the surface transmission coil employed.

DISCUSSION

As with the BISS8 pulse, the ASSESS pulse overcomes the disadvantages of 1D ISIS and the GMAX methods, which require motion-sensitive subtraction of two scans. The ASSESS pulse has advantages over the BISS8 pulse in that no segmentation of pulses is needed in its implementation. Compared to the BISS8 pulse, which requires abrupt switching of gradient polarity at its maximum strength, the ASSESS pulse places less demand on gradient performance. In this study, we are limited by the maximum gradient strength of our current hardware (6.7 mT/m). The slice thickness of the ASSESS pulse is inversely proportional to the peak gradient strength. A much thinner (than 2.7 cm) slice can be readily obtained with higher gradient strength available in small-bore spectrometers and increasingly available on whole-body human systems. The other advantage of the ASSESS pulse is that it uses half the pulse duration and deposits half of the RF power required by the BISS8 pulse under the same experimental conditions. This obviously extends the scope of practical applications of adiabatic slice-selective excitation pulses, particularly for human studies. The disadvantage of the ASSESS pulse is the perturbation of magnetization outside the selected slice and the limitation of slice selection to mainly equilibrium magnetizations.

When the gradient polarity of the second and the third segments of ASSESS pulses is reversed, a genuine slice-selective universal rotator pulse (mASSESS) is obtained. However, the nonzero chemical-shift offset and B_0 inhomogeneity are not refocused with this approach, which limits the practical applications of the mASSESS pulse. Exploring the symmetry properties of the ASSESS pulse, subtraction of two scans with proper change of flip angle in the second scan produces complete suppression of outer magnetization independent of B_0, B_1 homogeneity, and chemical-shift offset. This method is of advantage over the subtraction methods such as 1D ISIS or GMAX when the selected slice or volume is small compared to the total volume excited by the coil. The 1D ISIS and GMAX methods require extracting small differences from two large signals, putting high demand on the dynamic range of the ADC and restricting the receiver gain setting from obtaining the optimal signal-to-noise ratio. In contrast, by using the ASSESS pulse, outer-volume signals are greatly suppressed in each scan before subtraction.

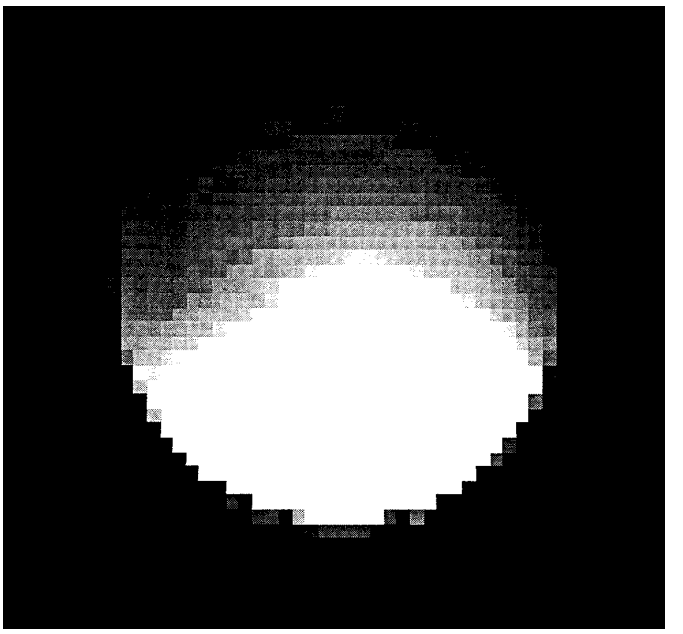

FIG. 11. Two-dimensional gradient-echo in-slice image of the same phantom obtained with the ASSESS pulse shown in Fig. 2. Similar experimental parameters as described in the legend to Fig. 10 were employed.

Although only a 90° ASSESS pulse is described here, the general results apply to excitation of arbitrary flip angles. Other flip angles can also be generated, as is true for a BISS8 pulse and a conventional BIR4 pulse. The fact that a zero-degree ASSESS pulse suppresses magnetization outside the selected slice while keeping the magnetization inside the slice intact immediately suggests its applications in many localization techniques. For example, our preliminary results have shown that a single-shot, adiabatic, three-dimensional localization using surface coils is possible with a succession of three ASSESS pulses with flip angles of 0°, 0°, and 90° on three orthogonal axes, respectively. STEAM and PRESS methods using ASSESS pulses are also possible. Such studies are currently in progress.

In conclusion, the ASSESS pulse achieves single-shot, adiabatic, slice-selective, pure-phase, self-refocused spin rotations of arbitrary flip angles using surface coils for RF transmission despite the presence of high B_1 inhomogeneity. Advantage is taken of the B_1 inhomogeneity produced by surface coils to obtain slice selection or outer-volume suppression. The relatively low RF power deposition, easy implementation, and short pulse duration as compared to the BISS8 pulse should extend the scope of applications of adiabatic slice-selective excitation to *in vivo* NMR studies using surface coils.

ACKNOWLEDGMENTS

We thank Dr. Robert E. Rycyna for help in implementation of the ParaVision software which was used for data acquisition and processing in this study, and Terry Nixon for improvements to and maintenance of the spectrometer. We also thank Professor Robert G. Shulman for advice, support, and helpful suggestions. This work was supported by a NIH First Award (R29 NS32126-02) to D. L. Rothman, and NIH Grants R01 EY10856-02 and R01 DK27121-16 to R. G. Shulman.

REFERENCES

1. M. S. Silver, R. I. Joseph, C.-N. Chen, V. J. Sank, and D. I. Hoult, *Nature* **310,** 681 (1984).
2. S. Conolly, D. Nishimura, and A. Macovski, *J. Magn. Reson.* **83,** 324 (1989).
3. K. Ugurbil, M., Garwood, and A. R. Rath, *J. Magn. Reson.* **80,** 448 (1988).
4. J. Shen, *J. Magn. Reson. B* **112,** 131 (1996).
5. K. Ugurbil, M., Garwood, A. R. Rath, and M. R. Bendall, *J. Magn. Reson.* **78,** 472 (1988).
6. M. Garwood and Y. Ke, *J. Magn. Reson.* **94,** 511 (1991).
7. J. Baum, R. Tycko, and A. Pines, *J. Chem. Phys.* **79,** 4643 (1983).
8. A. J. Johnson, M. Garwood, and K. Uğurbil, *J. Magn. Reson.* **81,** 653 (1989).
9. M. Saranathan and M. Kushmerick, *J. Magn. Reson. B* **110,** 69 (1996).
10. G. Morris and R. Freeman, *J. Magn. Reson.* **29,** 433 (1978).
11. R. A. de Graaf, K. Nicolay, and M. Garwood, *Magn. Reson. Med.* **35,** 652 (1996).
12. J. Baum, R. Tycko, and A. Pines, *Phys. Rev. A* **32,** 3435 (1985).
13. B. Blümich and W. Spiess, *J. Magn. Reson.* **61,** 356 (1985).
14. M. Shinnar and J. S. Leigh, *J. Magn. Reson.* **75,** 502 (1987).
15. L. Emsley and G. Bodenhausen, *Chem. Phys. Lett.* **168,** 297 (1990).
16. S. Conolly, D. Nishimura, and A. Macovski, *J. Magn. Reson.* **78,** 440 (1988).